NRC Publications Archive
Archives des publications du CNRC

Analysis of uncertainties in instantaneous soot volume fraction measurements using two-dimensional, auto-compensating, laser induced incandescence (2D-AC-LII)
Crosland, B.M.; Johnson, M.R.; Thomson, K.A.

National Research Council Canada
Conseil national de recherches Canada

Canada

Analysis of uncertainties in instantaneous soot volume fraction measurements using two-dimensional, auto-compensating, laser-induced incandescence (2D-AC-LII)

B.M. Crosland · M.R. Johnson · K.A. Thomson

Abstract Laser-induced incandescence (LII) is an optical measurement technique capable of measuring soot volume fraction over a wide range of conditions. However, development of two-dimensional auto-compensating LII (2D-AC-LII) in the literature has been limited and until now, instantaneous measurements have not been demonstrated. In this paper, we successfully demonstrate instantaneous 2D-AC-LII soot volume fraction (SVF) measurements in an ethylene-air co-annular diffusion flame. Results were then used to support a detailed uncertainty analysis based on a Monte-Carlo simulation. Agreement between both the instantaneous and average SVF measurements with published data from attenuation measurements under identical conditions was found to be good. Uncertainties are discussed both in terms of an overall accuracy of the SVF measurement, which is strongly dominated by uncertainty in the optical properties of soot, and the comparative uncertainties with optical properties fixed. The uncertainty in an instantaneous 2D determination of SVF for a comparative measurement is dominated by photon shot noise, and in regions of high soot volume fraction it is below 25% (95% confidence interval). Shot noise uncertainty could be further reduced with additional

pixel averaging at the expense of spatial resolution. This diagnostic shows significant promise for quantitative planar soot concentration measurements within turbulent flames.

1 Introduction

As a component of particulate matter, soot is a regulated pollutant that is closely linked with significant adverse health effects on humans [1] and climate forcing [2]. Accurate quantification of soot is vitally important both in the fundamental understanding of its formation mechanisms and in the quantification of emissions from flames and practical combustion devices.

Laser-induced incandescence (LII) measurement is an emergent optical combustion diagnostic, which can be used to determine the volume fraction and primary particle size distribution of soot [3–9]. In this technique, a laser pulse is used to heat soot aerosols to or close to their vaporization temperature. The incandescence signature from the soot is intense and short-lived, as the particles rapidly cool to the ambient temperature principally through conductive cooling and in some cases sublimation. The emission intensity is proportional to the concentration of the soot, but it is also highly dependent on the soot temperature. This temperature dependence can be used to advantage when the decay of the incandescence is measured as a function of time and used to predict the active surface area or effective primary particle size of the soot aggregates [6–9]. Conversely, the temperature dependence presents a challenge when trying to infer the particle concentration from the emission intensity, especially if the initial temperature of the soot before heating is unknown.

Two distinct strategies exist to overcome the temperature dependence of the measured emission. The first, often referred to as high-fluence or 'plateau-regime' LII [4, 10–12],

B.M. Crosland · M.R. Johnson
Department of Mechanical and Aerospace Engineering, Carleton University, Ottawa, Ontario, Canada K1S 5B6

B.M. Crosland
e-mail: BCroslan@connect.carleton.ca

M.R. Johnson
e-mail: Matthew_Johnson@carleton.ca

K.A. Thomson (✉)
National Research Council of Canada, Ottawa, Ontario, Canada K1A 0R6
e-mail: Kevin.Thomson@nrc-cnrc.gc.ca
Fax: +1-613-9577869

involves imparting sufficient energy to the particles to ensure they reach a sublimation temperature of 4000 to 4500 K independent of their initial temperature, thus ensuring a spatially-uniform soot temperature distribution. Under this condition, a near-proportionality of emission intensity and concentration is assumed to exist when comparing soot from different locations in a flame or indeed different sources [13, 14]. Plateau-regime LII requires calibration by comparing LII emission measurements to results from another calibrated technique (e.g. extinction measurements as in [15–18], or cavity ring-down spectroscopy as in [19–22]). These secondary techniques are either applied simultaneously or are used to quantify soot volume fraction in a reference flame that is subsequently used to calibrate the LII measurement.

The second strategy involves measurement of the temperature of the heated soot in real-time by two-color emission pyrometry [9, 23–25]. Since the temperature of the soot is explicitly calculated based on measurements, it is not necessary to reach sublimation temperatures, and thus the diagnostic is less intrusive and less sensitive to in-flame laser attenuation [23]. Measurement of incandescence intensity shortly after the laser pulse is used to determine soot concentration while the temperature decay is used to determine soot morphology. The method is referred to interchangeably as auto-compensating or two-color LII (2C-LII). We use auto-compensating LII (AC-LII) here to avoid confusion with another LII variant by Schoemaecker-Moreau et al. also named 2C-LII [26], which involves two laser wavelengths. AC-LII offers the significant advantage that calibration does not require comparison to other soot concentration diagnostics or to flames of known concentration. The method is also better suited for morphology measurement, since high-fluence LII has been demonstrated to significantly alter the interrogated soot [27].

Although development and application of AC-LII is progressing rapidly (e.g. [25, 28, 29]), including the use of single point AC-LII to calibrate simultaneous 2D-LII measurements [30], two-dimensional auto-compensating LII (2D-AC-LII) has received little attention to date [29] and has yet to be demonstrated as an instantaneous measurement technique. Specifically, there remain significant challenges for the design and demonstration of an optical system which provides an optimal laser excitation and sufficient sensitivity throughout the measurement field-of-view to permit single shot data acquisition. In this paper we present a 2D-AC-LII apparatus and quantitatively evaluate its potential for instantaneous planar measurements of soot concentration. The system is demonstrated on a laminar co-annular ethylene/air non-premixed flame to permit direct, critical comparison of results with data from other sources. Detailed uncertainty limits are also analyzed and discussed. This proposed approach shows significant promise for quantitative planar soot concentration measurements within turbulent flames.

2 Theory

The underlying principle of AC-LII is two-color pyrometry. Soot temperature is first determined by the ratio of emission intensity at two wavelengths and soot concentration is determined from comparison of the absolute emission intensity at either measurement wavelength and the theoretical emission intensity per unit volume of soot at the measurement temperature.

The theoretical emission per unit volume of soot at temperature T_p and at wavelength λ is [23]:

$$\phi_P(\lambda, T_p) = \frac{48\pi^2 c^2 h}{\lambda^6} \left[\exp\left(\frac{hc}{k\lambda T_p}\right) - 1 \right]^{-1} E(m_\lambda) \quad (1)$$

where c is the speed of light, h is Planck's constant, k is the Stefan-Boltzmann constant and $E(m_\lambda)$ is the wavelength-dependent soot absorption function. Recognizing that practical detectors measure an integration of signal over a finite spectral range, I_i, the signal measured by the intensified charge-coupled device (ICCD) on channel i is then:

$$I_i = f_v \left(M_i^2 A_p w_b\right)\left(A_L/u_i^2\right)\alpha_i\beta_i$$
$$\times \int_\lambda \phi_P(\lambda, T_p)\Omega_i(\lambda)\,d\lambda + D_i \quad (2)$$

where f_v is the volume fraction of soot, w_b is the laser sheet thickness, D_i is the ICCD dark count and $\Omega_i(\lambda) = \tau_i(\lambda)\Theta_i(\lambda)$, for which $\tau_i(\lambda)$ is the product of the optical transmissivities of the lens and filters and $\Theta_i(\lambda)$ is the photocathode responsivity, both of which can be determined from manufacturers' specifications. It should be noted that even for the present case of soot measurements within an ethylene diffusion flame, the contribution of flame luminosity was determined to be negligible compared to the LII signal. This leaves only wavelength-independent terms relating to the detector package including: magnification of the collection optics, M_i; area of a CCD pixel, A_p; area of the camera lens, A_L; distance between the lens and the laser sheet, u_i; intensifier gain, α_i; and CCD gain, β_i, which are hereafter grouped into a single term, η_i. The coefficient η_i can be determined from a calibration of the optical system using a radiant standard placed coincident with the measurement location according to:

$$I_{\text{lamp},i} = \eta_i 4\pi \int_\lambda R_s(\lambda)\Omega_i(\lambda)\,d\lambda + D_{i,\text{lamp}} \quad (3)$$

where $R_s(\lambda)$ is the spectral radiance of the calibrated source, and $I_{\text{lamp},i}$ is the measured signal during calibration and $D_{\text{lamp},i}$ is the dark count measured with the intensifier off but the lamp on. This latter term is especially important in correcting for leakage through the photocathode during calibration, since the lamp provides a continuous signal and the

CCD readout time is long compared to the intensifier gate width. This calibration is performed for each pixel on the CCD to generate a spatially-variant pixel sensitivity map, $\eta_{i,x,y}$.

The ratio of LII signals from the two wavelength ranges corresponding to the two measurement channels provides an expression:

$$I_1/I_2 = \eta_1 \int_\lambda \phi_p(\lambda, T_p) \cdot \Omega_1(\lambda) d\lambda$$
$$\times \left(\eta_2 \int_\lambda \phi_p(\lambda, T_p) \cdot \Omega_2(\lambda) \, d\lambda \right)^{-1} \quad (4)$$

where f_v and w_b cancel in the ratio and temperature is the only unknown. However, determination of T_p is computationally intensive. Snelling et al. [23, 28] propose an 'equivalent filter' method that allows (4) to be reformulated into an explicit expression from which T_p is easily determined. To avoid this approximation while maintaining a fast data processing algorithm, we instead pre-compute the RHS of (4) for a range of T_p and develop a look-up table of $T_p = $ fn(I_1/I_2). Once T_p has been determined, f_v can be solved by (2), using the measured LII signal from either measurement channel.

To account for the Gaussian intensity profile of the laser sheet used in this study, where soot will not be uniformly heated to a single peak temperature, an equivalent temperature and sheet thickness method [23] can be used. In this case, the soot temperature calculated using (5) will only be an *equivalent* temperature (T_e), and thus requires a corresponding *equivalent* laser thickness (w_e), which by definition is the thickness that will yield a correct soot volume fraction when used with the equivalent temperature in (2) [23]. The impacts of this approach on measurement uncertainty are considered in the overall uncertainty analysis discussed later.

An appropriate equivalent laser thickness for the current laser sheet profile and peak fluence (1.3 mJ/mm^2, $\lambda =$ 1064 nm) was determined via numerical simulation of the LII process using the method described in [23]. Sublimation was not considered in the simulation because of the low fluences involved. Example simulation results for three primary particle diameters and three peak laser fluences are shown in Fig. 1.

After strong variation immediately following the laser pulse, the equivalent width remains quite stable over the ICCD gate period from 20 to 60 ns. This is helpful both in reducing sensitivity to timing between the laser and the ICCD and in keeping the formulation of the soot volume fraction equations independent of time. Furthermore, variation in w_e with primary particle diameter is negligible and modest with peak laser fluence.
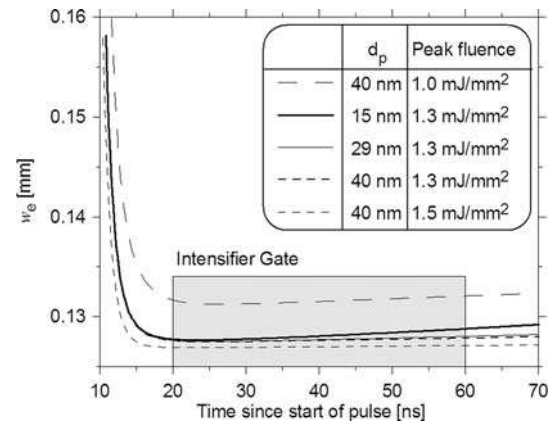

Fig. 1 The required equivalent sheet thickness remains relatively uniform during the intensifier gate

Beam steering is an important issue to consider when applying optical diagnostics in flames. Distortion of the excitation laser due to refractive index gradients have been shown to be a problem in high pressure test rigs but was found to be less significant at atmospheric pressure [31]. In the present case, the laser is passed through the centerline of an axisymmetric flame and thus normal to the temperature and refractive index gradients and therefore negligible distortion of the laser beam is anticipated. Beam steering can also influence the emitted incandescent signal in the form of image blurring where the largest steering occurs in regions of low temperature and high temperature gradient, or outside of the soot region of the present flame. Within the sooting zone, beam steering is expected to be quite small other than near the burner exit [32].

3 Equipment

A schematic of the experimental apparatus is shown in Fig. 2. The output of a pulsed Nd:YAG laser (Litron Lasers Ltd., LPY-642T-10) operating at 1064 nm and a pulse width of about 10 ns was focused into a sheet using a Powell lens (Laser Line Generator, StockerYale Canada). The laser fluence was adjusted using a half-wave plate and thin-film polarizer. The sheet had a near-uniform profile over its 4 cm height and a Gaussian profile through the waist with a full-width, half-maximum thickness of 130 μm. The peak fluence of the sheet was approximately 1.3 mJ/mm^2, determined using a beam profile camera (Coherent Inc., LaserCam-HR) and a power meter (Scientech Inc.).

A pair of 16-bit PI-MAX ICCD cameras (Princeton Instruments) were fitted with 180 mm, f/# 3.5 macro camera lenses (Sigma Corporation). The ICCDs differed only in their wavelength optimizations. The ICCDs were fitted with bandpass filters (Semrock Inc.) with center wavelengths of 442 nm and 684 nm and bandwidths of 46 nm and 24 nm,

respectively. A dichroic beamsplitter (BMV Optical Technologies) was used to split the LII emission normal to the laser sheet from a height of 22 mm to 39 mm above the burner exit onto the two ICCDs. The magnification was 0.9, with one pixel representing 22.2×22.2 μm; however, images were binned horizontally and vertically by 5 pixels in order to improve signal-to-noise. The spectral transmissivity of the filters and beamsplitter and the quantum efficiency of the intensifiers were provided by the manufacturers.

A NIST-traceable 4″ integrating sphere and tungsten filament lamp (SphereOptics LLC) calibrated as a unit to provide a source of radiant intensity, uniform to 1% over the exit port of the sphere, was used to determine $\eta_{i,x,y}$ for both IC-CDs. The spectral radiance of the sphere was monitored using a spectrometer calibrated by SphereOptics for use with the sphere. During calibration, multiple images were averaged to reduce the photon shot noise uncertainty to 2.5% of the mean signal. The integrating sphere was also used to determine the ICCD gain using photon transfer theory [33]. This allowed the photon shot noise in a given instantaneous measurement to be approximated and allowed verification

that photon shot noise was the dominant source of noise over all of the selected operating range. An average image of the exit port of the sphere was acquired with the intensifier disabled to be subtracted as $D_{i,\mathrm{lamp}}$. All acquired images were spatially calibrated and correlated (registered) between the ICCDs by acquiring images of a rectangular grid of 0.75 mm diameter circles, spaced 1.10 mm apart, and applying a commercial spatial calibration and pixel registration algorithm *DaVis* (LaVision GmbH).

Measurements were performed on a Gülder burner ethylene/air flame described in [34] for the standard operating conditions of 194 sccm ethylene (1 atm, 21°C) and 284 slpm co-flow air. This is a stable and repeatable flame for which detailed measured soot volume fraction data were available [35].

4 Results

Figure 3 summarizes the key measurement results. In Fig. 3a, T_e determined from the ratio of a single shot image pair is shown. Figure 3b is the corresponding instantaneous f_v, while Fig. 3c is the 100-image averaged soot volume fraction. Two-dimensional line-of-sight attenuation (2D-LOSA) measurements of soot volume fraction [35], are included in Fig. 3d for comparison. As will be discussed in the uncertainty analysis below, the results obtained via 2D-AC-LII are expected to underestimate the soot volume fraction by as much as 5% due to soot cooling during measurement.

The equivalent temperatures shown in Fig. 3a range from 2700 K between $y/R = 5$ to $y/R = 7$, and $r/R = \pm 0.4$ to a maximum of approximately 3900 K at isolate points near $r/R = -0.55$ and $y/R \approx 4.7$. The temperatures in Fig. 3a are all below the LII plateau regime, which nominally begins at temperatures of approximately 4000–4500 K [14, 28, 36]. Comparing the left and right peaks of equivalent temperature from $y/R = 4.5$ to $y/R = 6.5$, the right peak is, on
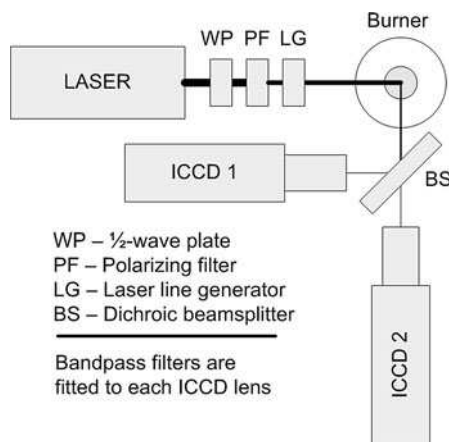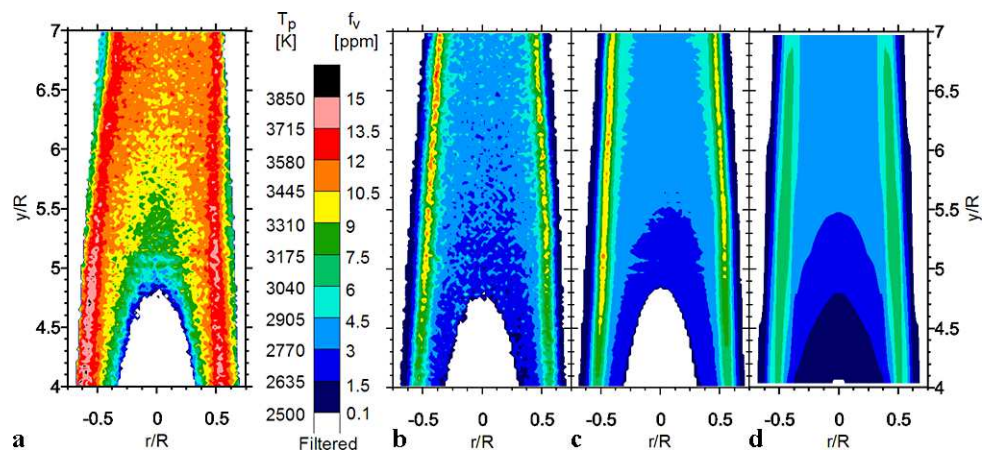

Fig. 2 Schematic of the experimental apparatus

Fig. 3 (**a**) Equivalent temperature and soot volume fraction as measured instantaneously via (**b**) 2D-AC-LII, (**c**) by average of 2D-AC-LII measurements, and (**d**) by 2D-LOSA [35]. The fuel tube radius, $R = 5.45$ mm
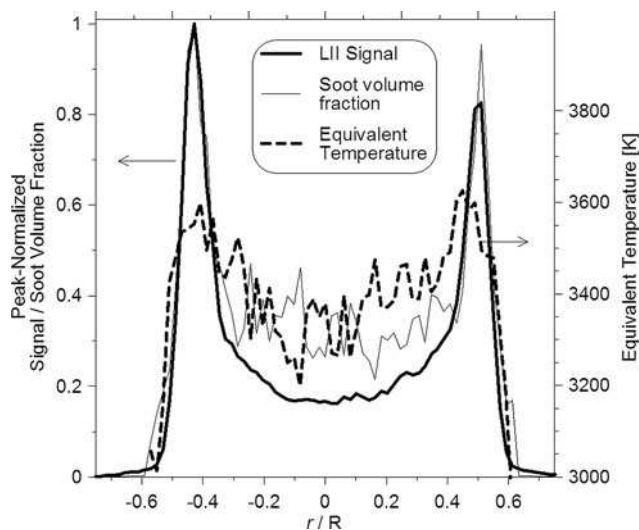
Fig. 4 Accounting for variations in soot temperature compensates for decreased laser fluence at the right-hand soot peak

average, 90 K lower than the left due to laser sheet attenuation from soot. The effect of laser attenuation on the LII signal can be seen in Fig. 4, where the LII signal peaks are not equal. The soot volume fraction, however, is near-symmetric due to the incorporation of a spatially-varying temperature term in its calculation. This result highlights the importance of correcting for spatial variation of temperature in 2D-LII and reveals a potential advantage of the present approach over single point or reference flame calibrations, for which laser attenuation must be overcome by operating well above the sublimation threshold.

5 Discussion and analysis of uncertainty

The propagation of uncertainty from elemental sources of error through to the soot volume fraction calculation was performed via Monte-Carlo simulation. Repeated calculations of soot volume fraction were made at each point in the measurement volume using values randomly selected from appropriate probability distributions accounting for the individual uncertainties of each term in (2). This yields a sample of soot volume fractions whose normalized histogram approximately represents the probability density function of the soot volume fraction at that point. The sample was considered converged when the half-width of the 99% confidence interval of the mean soot volume fraction was found to be less than 1% of the sample mean soot volume fraction. Unbiased estimates of the confidence intervals used to determine convergence are obtained using the method of [37].

5.1 Calibration uncertainties

The first source of uncertainty arises during the calibration of the ICCDs. Calibration was accomplished using a

tungsten filament lamp irradiating a 4″ diameter integrating sphere. The uncertainty of the NIST standard and the transfer uncertainty (from the NIST standard to the spectrometer) were provided by the manufacturer of the spectrometer. Multiple spectra were obtained and averaged, and the variation between measurements was added to the NIST standard and the transfer uncertainties as the root of the sum of the squares. For the purposes of the uncertainty analysis the spectral radiance was assumed not to vary as a function of wavelength within the relatively narrow range of each bandpass filter.

Simultaneous with the acquisition of spectra using the spectrometer, multiple images of the sphere output were obtained with each ICCD using the same experimental parameters (f/#, intensifier gate width, ICCD placement and frame rate) that were used later during LII measurements. Photons emitted by the lamp traveled through the integrating sphere, passed through the beamsplitter, filter, and camera lens, struck the image intensifier, and induced an intensified signal on the CCD. The beamsplitter, filter, camera lens and intensifier photocathode are all wavelength-dependent devices. Though the nominal values of the wavelength-dependent transmissivities, $\Omega_i(\lambda)$, were known, their uncertainties were not. However, by calibrating the cameras and performing the data gathering with an identical optical arrangement any uncertainties that are independent of wavelength cancel [23]. Furthermore, any uncertainties that vary linearly with wavelength cancel to a first-order approximation, if the lamp and soot emission signals also vary linearly with wavelength over the relatively narrow width of each filter. The robustness of this approach was verified by an analytical simulation, which revealed that a rather extreme wavelength-dependent variation of 20% in the system transmissivity over the filter bandwidth produced a change of less than 1% in the calibration. Thus, uncertainties in the component transmissivities of the collection optics were considered negligible. It is noted that this result also explains why the "equivalent filter" approximation [23] works well.

The uncertainty in the ICCD calibration signal, I_{lamp}, is dominated by inherent randomness of the emitted photons. Because the gate width of the intensifier is short, the random nature of photon emission has a non-negligible effect on the final image, known as photon shot noise. Since it is known that photon shot noise follows a Poisson distribution, it is possible to determine the approximate camera gain in counts/e$^-$ using a sensitivity-corrected flat-field image, which in turn can be used to approximate the photon shot noise in a measured signal [33].

Photon shot noise was verified to be the dominant source of uncertainty in the range of signals used for calibration. Since the dark count (D_{lamp}) was small relative to the calibration signal, any uncertainty in the subtracted dark count was negligible relative to the uncertainty in the calibration

signal itself. The total uncertainty in the calibration constant, $\eta_{i,x,y}$, was thus reduced to the contributions of the uncertainty in the spectrometer and the photon shot noise inherent in the lamp signal. Since the calibration signal was made up of the photon count amplified by a gain, a Poisson distribution should be used to represent it. However, the mean signal was large enough relative to its standard deviation that a normal distribution could be used with negligible risk of randomly selecting a negative calibration signal. For this reason, and to simplify coding, normal distributions were thus used for all shot noise dominated uncertainty.

5.2 Uncertainties during data collection

The uncertainty in the equivalent sheet thickness calculation arises from the assumptions inherent in the numerical model, which relate to imperfect knowledge of the laser profile, laser fluence, and soot optical properties. It is difficult to assess the accuracy of the numerical model alone, since this would require determination of the accuracy of the LII model, which is beyond the scope of this work, and is indeed an open question in the literature. However, it is possible to estimate the overall uncertainty associated with using the equivalent sheet thickness approximation by considering a wide range of potential values for the relevant experimental parameters and soot properties used in the model to determine a range of possible equivalent sheet widths. Given that the uncertainties in optical properties dominate the overall uncertainties as noted below, such an approach will also encompass the range of sheet widths that would result from the inaccuracies of the model itself.

Parametric simulations of the LII process were performed to facilitate statistical sampling during Monte-Carlo simulations necessary to calculate overall uncertainties. The range of possible values of the soot absorption function ($E(m)_\lambda$) and the ratio between the $E(m)$ values at the two detection wavelengths were chosen to slightly exceed the nominal ranges derived from data reported in the literature [38–41], to permit sampling from a Gaussian distribution profile. For each value of $E(m)_1$ ranging from 0.27 to 0.41 in increments of 0.02, four values of $E(m)_2$ were tested based on a range of potential wavelength dependencies of $E(m)_\lambda$ prescribed as the ratio, $\varphi = E(m)_1/E(m)_2$ which had assigned values of 0.8, 0.9, 1.0 and 1.1. Additionally, for each pair of $E(m)_1$ and φ tested, a probability distribution of equivalent sheet width thickness was determined based on a range of peak laser fluences ($F_L = 1.0$–1.6 mJ/mm^2) primary particle diameters ($d_p = 15$–40 nm) and thermal accommodation coefficients ($\alpha = 0.20$–0.50). During the Monte-Carlo simulation, this library of probability distributions was used to select an appropriate random equivalent sheet width based on randomly selected $E(m)_1$ and φ. The same $E(m)_1$ and φ pair was also used in the subsequent determination of the

soot equivalent temperature and the soot volume fraction. As noted by Liu et al. [42], although the uncertainties in the values of $E(m)$ at the two detection wavelengths each contribute to the overall uncertainty in the measured soot volume fraction, the relative contributions to the overall uncertainty can vary. Similarly, depending on how the uncertainties in $E(m)$ may vary with wavelength, a slightly different *estimate* of the overall uncertainty in soot volume fraction can be derived depending on which of the two detector signals is used in the final calculation of f_v, following the calculation of temperature. However, the calculated f_v and the *true* uncertainty of f_v (which is not determinable) are not affected by the choice of image used to determine f_v and so there is no advantage in choosing one signal wavelength over the other.

Photon shot noise remained the dominant source of uncertainty in LII emission measurements over the range of measured intensities. As was true during calibration, the uncertainty in the dark count was negligible compared to the uncertainty in the measured signal from photon shot noise. Thus the uncertainty in the measured signal, $I_i - B_i$, was based on the magnitude of the measured signal alone, converted into photons via the measured system gain. Once again, uncertainties related to the collection optics canceled out between calibration and data measurement.

The effects of photon shot noise during LII measurements contributed not only to the uncertainty of the soot volume fraction directly via the I term in (2), but also comprised a significant component of the uncertainty in the determination of the equivalent temperature (T_e). To decrease this uncertainty in an instantaneous measurement more photons must strike the photocathode of the intensifier or adjacent pixels must be binned during post-processing. More photons can be collected by making any of a number of changes to the experimental setup, including using a faster lens arrangement (lower f-number), increasing the intensifier gate width (thus increasing the bias error due to particle cooling during measurement), or using a thicker laser sheet (thus sacrificing spatial resolution in this direction). Binning adjacent pixels during post-processing decreases the spatial resolution in the plane of the image but also increases signal-to-noise by the square root of the number of binned pixels. In the current measurements the spatial resolution perpendicular to the plane of the image (represented by the laser sheet thickness) was greater than the spatial resolution represented by a single pixel width, making binning the preferable first choice for reducing photon shot noise uncertainty. As mentioned previously, all LII data presented here resulted from a binning of 5×5 pixels during analysis.

The non-linearity of an individual pixel's response to incident photons is considered negligible in the range used for the current measurement (less than 20% of the CCD full-well capacity). If this were not the case, a simultaneous correction for CCD pixel response non-uniformity and

non-linear CCD response such as that proposed by Shaddix & Williams [43] could be employed. The non-uniform pixel response among pixels in the CCD array was corrected using a sensitivity map created during calibration with the tungsten filament lamp and integrating sphere.

The formulation of (1) implicitly assumes that the soot particle temperature does not change significantly during measurement. The shortest gate width possible with the ICCDs used is about 5 ns, which is not negligible relative to typical measured soot cooling rates in the range of 1–10 K/ns [28]. Thus the assumption of a constant temperature introduces a non-negligible bias error into the soot volume fraction calculation. The amount of bias introduced will depend on the soot cooling rate, the ICCD gate width and the soot temperature. Because the cooling rate will differ temporally and spatially, as well as from one flame to another, it would be a challenge to correct for the cooling rate without performing complementary time-resolved measurements. The bias introduced by a range of cooling rates using the present apparatus was approximated by simulating an LII signal created by a given volume of soot cooling at a constant rate and calculating soot volume fraction based solely on the time-integral of this signal. Results for a range of cooling rates beginning at two initial temperatures (T_0) and using three gate widths are presented in Fig. 5.

The current research used a gate width of 40 ns as a compromise between a stronger signal (decreasing photon shot noise) and an increased gate width bias error. Because the cooling rate is not precisely known for most flames it is difficult to account for it in the uncertainty analysis. However, the bias error for the current results should be less than about 5% (Fig. 5, hollow square, highest cooling rate), which is not a significant factor in the overall uncertainty as will be shown below.

Another bias error is introduced via the absorption of the soot incandescence signal by soot located between the measurement volume and the detector, an effect known as signal trapping. Though corrections for signal trapping exist based on Bouguer's law, they all require knowledge of the soot concentration between the measurement volume and the detector. Since this information would not be available for instantaneous measurements of an unsteady flame, it is treated as an unknown bias uncertainty. Since lower wavelengths are preferentially absorbed, the heated soot temperature inferred via pyrometry will be underestimated, often resulting in the overestimation of soot volume fraction [44–46]. Recent work by [44] indicates that the underestimation of the temperature combined with the decreased signal intensity causes overestimation of soot volume fraction by 17% or less for the flame studied here. As with the underestimation due to the non-zero gate width bias error, this is a limit on the maximum expected error and is not considered to be significant to the overall uncertainty.

5.3 Uncertainties of instantaneous and mean f_v measurements using 2D-AC-LII

A summary of the probability distributions used in the random sampling of variables for the Monte-Carlo analysis is provided in Table 1. The final measurement uncertainty at each location in the flame was determined via analysis of the soot volume fraction histograms produced by the Monte-Carlo simulation. To distinguish between the total measure-
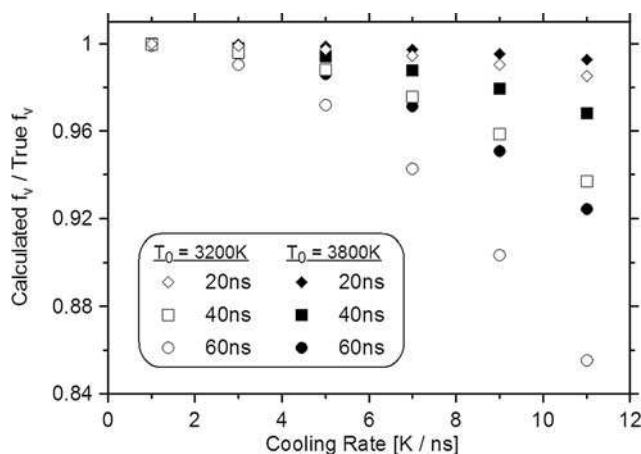

Fig. 5 The non-zero gate width bias error for the current measurement system

Table 1 Summary of distributions used as inputs for the Monte-Carlo simulation

| Variable	Distribution	Parameters		Units
Variables used in (1) *and* (2)				
$R_s(\lambda_1)$	Normal	$\mu = 182$	$\sigma = 2.7$	W/(cm^2 nm)
$R_s(\lambda_2)$	Normal	$\mu = 974$	$\sigma = 8.3$	W/(cm^2 nm)
$\Omega(\lambda)$	1st order negligible	–	–	–
$I_{\text{lamp},1}$	Normal	$\mu = 1061$	$\sigma = 2.8$	ADU
$I_{\text{lamp},2}$	Normal	$\mu = 1233$	$\sigma = 4.5$	ADU
$D_{\text{lamp},1}$	Negligible	–	–	–
$D_{\text{lamp},2}$	Negligible	–	–	–
I_1	Normal	Measured	f (gain)	ADU
I_2	Normal	Measured	f (gain)	ADU
B_1	Negligible	–	–	–
B_2	Negligible	–	–	–
$E(m)_1$	Normal	$\mu = 0.32$	$\sigma = 0.023$	–
φ	Normal	$\mu = 0.99$	$\sigma = 0.056$	–
ω_e	Custom	$E(m)_1, E(m)_2, \alpha, d_p, F_L$		mm
Variables specific to the equivalent sheet width calculation				
F_L	Uniform	Min 1.0	Max 1.6	mJ/mm^2
d_p	Uniform	Min $= 15$	Max $= 40$	nm
α	Uniform	Min $= 0.20$	Max $= 0.50$	–
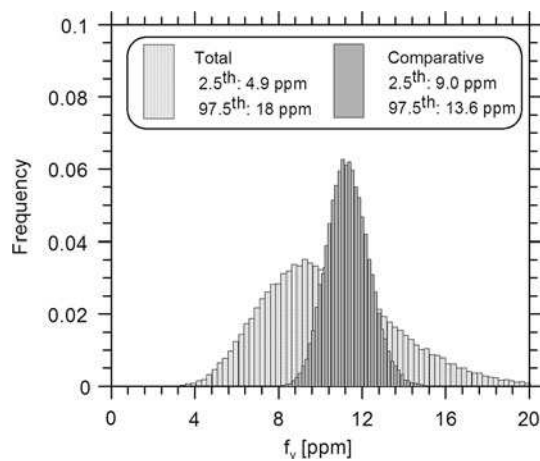
Fig. 6 Histograms of soot volume fraction in a strongly sooting region
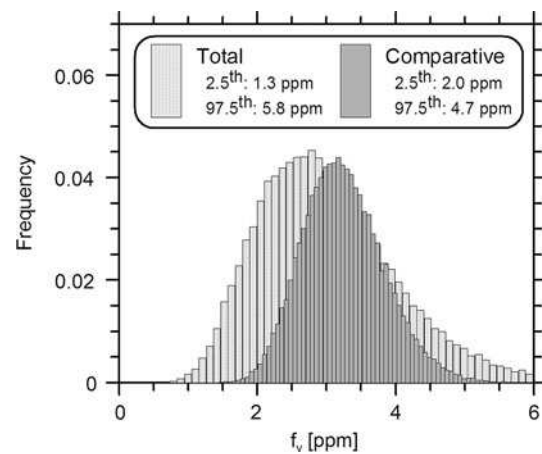

Fig. 7 Histograms of soot volume fraction in a weakly sooting region

ment uncertainty (i.e. including uncertainties in soot properties common to all similar optical techniques) and the uncertainty specific to the diagnostic (i.e. the uncertainty that would be apparent in comparative measurements using the same diagnostic), Monte-Carlo simulations were performed under two distinct sets of conditions. During the first Monte-Carlo simulation all the terms in (2) were allowed to vary, producing histograms of soot volume fraction that incorporate the total measurement uncertainty. During the second Monte-Carlo simulation only those terms that vary from one single instantaneous measurement to the next were allowed to change. Thus terms which are imprecisely known from the literature such as the thermal accommodation coefficient and the soot absorption function were fixed at nominal values. This produces histograms incorporating only the error terms which are present when comparing one instantaneous measurement to another, referred to here as the comparative error. Example normalized histograms of measured soot volume fraction, taking into account the total error and the comparative error, are shown in Figs. 6 and 7 for a strongly and weakly sooting region of the flame respectively.

As expected, the uncertainty distributions are narrower when comparing two measurements with the 2D-AC-LII diagnostic than when considering the absolute magnitudes of the soot volume fraction. Also evident in Figs. 6 and 7 is the slight asymmetry of the uncertainty distributions themselves. The lower and upper limits of a 95% confidence interval are the 2.5 and 97.5 percentile of the calculated soot volume fractions distribution. Because the distribution is asymmetric, these limits are not equidistant from the mean soot volume fraction. For this reason the half-width relative to the mean (relative uncertainty) must be calculated separately for both the upper and lower limits of the confidence interval as is done in Fig. 8, which shows data for an instantaneous 2D-planar measurement of the soot volume fraction within an ethylene-air co-flow diffusion flame.

The total uncertainty is significantly greater than the comparative uncertainty through much of the flame. The uncertainty for a comparative measurement (Fig. 8d, e) falls to a minimum where the measured signal is at its maximum indicating that it is dominated by signal-to-noise associated with photon shot noise. By contrast, the uncertainty for an absolute measurement (Fig. 8b, c) varies less spatially, does not show a clear minimum at the region of maximum soot volume fraction, and has a larger contour of minimum uncertainty. This indicates the dominant uncertainty in an absolute measurement of the soot volume fraction is a state variable (e.g. optical properties of soot, laser sheet width or the equipment optical arrangement).

Although Fig. 9 shows that the shot noise uncertainty can be reduced with increased pixel binning, the effect is much stronger for a comparative than an absolute measurement, further confirming the importance of a state variable in determining the overall uncertainty. The uncertainty in a comparative measurement drops roughly as $N^{-1/2}$, where N is the number of pixels binned. Binning pixels into regions larger than 5×5 has no apparent benefit in reducing the overall uncertainty.

The sensitivity of the soot volume fraction to each of the variables in (2) can be shown as a scatter plot comparing the computed soot volume fractions and a variable of choice. This was done for all of the variables included in the Monte-Carlo analysis to assess the relative influence of each in determining the comparative and total uncertainties. An example plot relating the computed soot volume fraction to the intensity of the LII signal measured by channel 2 (I_2) for a sample location in the flame ($r/R = -0.39$, $y/R = 6.35$) is shown in Fig. 10. In this case, a weak correlation is observed between the total uncertainty in SVF and the uncertainty in I_2, while strong correlation is observed for the comparative uncertainty. This indicates the influence of the uncertainty in I_2 in each of the measures.
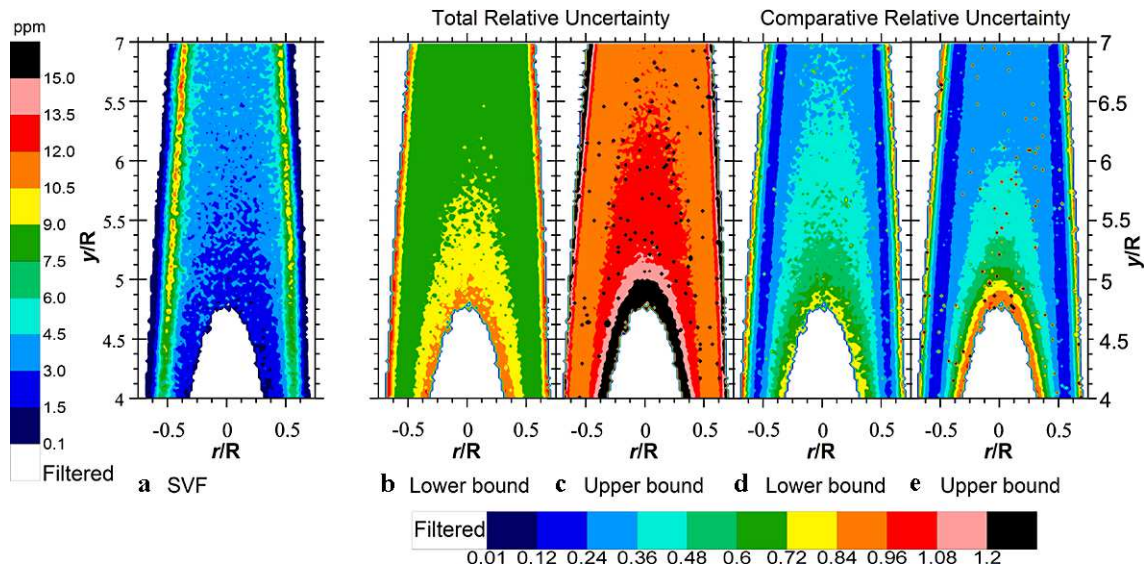
Fig. 8 An instantaneous 2D-planar measurement of the soot volume fraction (in parts per million, ppm) (**a**), as well as the upper and lower bounds of the 95% confidence intervals for the total uncertainty [(**b**) and (**c**)] and the comparative uncertainty [(**d**) and (**e**)]
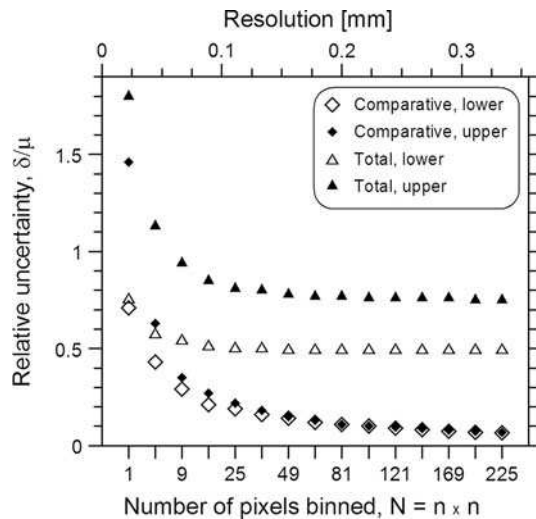

Fig. 9 The relative uncertainty as a function of pixel bin size for square bins

Fig. 10 Example scatter plots from the Monte-Carlo analysis showing the influence of the measured signal (I_2) in determining the (**a**) total uncertainty, and (**b**) comparative uncertainty in measured soot volume fraction. *Plotted lines* are linear least-squares fit to indicate the strength of the correlation

To permit comparison among the different input variables, the slopes of each linear least-squares fit line was multiplied by the standard deviation of the variable in question. For example, if I_1 were to increase by one standard deviation, the resultant soot volume fraction would decrease by 0.25 ppm. If I_2 were to increase by one standard deviation, the resultant soot volume fraction would increase by 0.7 ppm. Table 2 shows these sensitivities for two sample locations in the flame. Intermediary results such as w_e and T_p are included at the bottom of the table. Variables that were considered negligible (see Table 1 for a summary) were not included in Table 2.
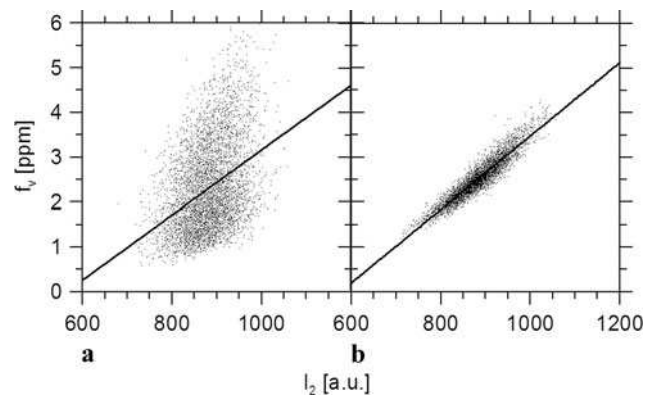
Results of the sensitivity analysis demonstrate that the total uncertainty is dominated by the uncertainty in the soot absorption function. This uncertainty strongly influences the intermediary calculations of equivalent width and equivalent soot temperature, which ultimately influence the measured soot volume fraction. Decreasing the photon shot noise via increased pixel binning would have little effect on the total uncertainty, both in strongly and weakly sooting regions since the I_1 and I_2 sensitivities are negligible compared to the φ sensitivity. The comparative uncertainty results indicate that increased signal on measurement channel 2, perhaps via a change in the filter bandwidth, would decrease the comparative uncertainty in both strongly and weakly sooting regions.

Table 2 Sensitivity of soot volume fraction (ppm per standard deviation of variable in question). The high soot data is at $r/R = -0.39$, $y/R = 6.35$, the low soot data $r/R = 0$, $y/R = 6.35$

Variable	Total		Comparative	
	High soot	Low soot	High soot	Low soot
f_v	10.2 ppm	2.9 ppm	10.2 ppm	2.9 ppm
Monte-Carlo input variables				
$R_s(\lambda_1)$	−0.30	−0.09	–	–
$R_s(\lambda_2)$	0.26	0.08	–	–
$I_{lamp,1}$	0.02	∼ 0	–	–
$I_{lamp,2}$	−0.04	∼ 0	–	–
I_1	−0.10	−0.06	−0.11	−0.06
I_2	0.29	0.17	0.32	0.18
$E(m)_1$	−0.47	−0.14	–	–
$\varphi = \frac{E(m)_1}{E(m)_2}$	2.54	0.733	–	–
Intermediate results derived using the above input variables				
w_e	−2.37	−0.67	–	–
T_p	−2.52	−0.73	−0.30	−0.19
η_1	0.30	0.09	–	–
η_2	−0.27	−0.08	–	–

The large total uncertainty and the strong dependence of soot volume fraction on soot optical properties are consistent with observations made previously in the literature for single point LII measurements. In [47] soot volume fraction results were plotted for a range of possible $E(m)$ slopes and it was found that soot volume fraction varied from −30% to 65% as the slope of $E(m)$ was varied over a realistic range. De Iullis et al. [24] noted the influence of $E(m)_\lambda$ in their data interpretation and inconsistencies between optimal choice for $E(m)_\lambda$ in LII and extinction measurements and suggested the need for a follow up investigation. Liu et al. [42] presented a formalized analysis of the sensitivity of soot temperature and concentration from auto-compensating LII and noted a strong dependence of soot volume fraction on $E(m)_1$ and $E(m)_2$. We can therefore only reiterate that accurate determination of the variation of the soot absorption function with wavelength is critical to the accuracy of auto-compensating LII. However, the comparative uncertainty analysis, which is the important uncertainty in experiments designed to measure and observe responses to controlled variation of input parameters, suggests the current implementation of 2D-AC-LII could be a valuable tool for understanding instantaneous soot formation in turbulent or time-varying flames. Furthermore, in situations amenable to ensemble averaging such as synchronized instantaneous realizations of in-cylinder reactions or of an acoustically forced flame, the comparative uncertainties could be further reduced via repeated measurements. In light of the significant challenges common to all optical diagnostics for measuring soot, the 2D-AC-LII technique is a significant development in the search for quantitative approaches to measuring instantaneous soot volume fractions in more than one dimension.

6 Conclusions

Instantaneous, 2D measurements of soot volume fraction have been successfully demonstrated in a co-annular ethylene diffusion flame. Measured results were used to perform a Monte Carlo simulation, which permitted a comprehensive determination of the total and comparative uncertainty in 2D-AC-LII measurements. The spectral variation of the soot refractive index absorption function, $E(m)_\lambda$, dominates the total measurement uncertainty because of its relatively high uncertainty and strong influence on the measured soot volume fraction. The comparative uncertainty, which fixes values of key optical properties and is the relevant uncertainty to consider when comparing between measurements, is strongly dependent on the photon shot noise present in the measured signal at the upper measurement wavelength. The calculation method has been shown to correct for laser sheet attenuation to within experimental uncertainty. With careful attention to experimental parameters and experimental uncertainty, instantaneous auto-compensating measurements of two-dimensional soot volume fraction could be achieved in turbulent flames in order to provide valuable information about the soot formation process.

References

1. USEPA, Integrated Science Assessment for Particulate Matter (External Review Draft), EPA/600/R-08/139, Washington, DC, 2008
2. IPCC, *Climate Change 2007: The Physical Science Basis. Contribution of Working Group I to the Fourth Assessment Report of the Intergovernmental Panel on Climate Change* (Cambridge University Press, Cambridge, 2007)
3. L. Melton, Appl. Opt. **23**, 13 (1984)
4. C. Schulz, B.F. Kock, M. Hofmann, H. Michelsen, S. Will, B. Bougie, R. Suntz, G. Smallwood, Appl. Phys. B **83**, 3 (2006)
5. H.A. Michelsen, F. Liu, B.F. Kock, H. Bladh, A. Boiarciuc, M. Charwath, T. Dreier, R. Hadef, M. Hofmann, J. Reimann, S. Will, P.-E. Bengtsson, H. Bockhorn, F. Foucher, K.-P. Geigle, C. Mounaïm-Rousselle, C. Schulz, R. Stirn, B. Tribalet, R. Suntz, Appl. Phys. B **87**, 3 (2007)
6. S. Will, S. Schraml, A. Leipertz, Opt. Lett. **20**, 22 (1995)
7. S. Schraml, S. Dankers, K. Bader, S. Will, A. Leipertz, Combust. Flame **120**, 4 (2000)
8. K.J. Daun, B.J. Stagg, F. Liu, G.J. Smallwood, D.R. Snelling, Appl. Phys. B **87**, 2 (2007)

9. B.F. Kock, B. Tribalet, C. Schulz, P. Roth, Combust. Flame **147**, 1 (2006)

10. T. Ni, J.A. Pinson, S. Gupta, R.J. Santoro, Appl. Opt. **34**, 30 (1995)

11. B. Axelsson, R. Collin, P.-E. Bengtsson, Appl. Opt. **39**, 21 (2000)

12. D.J. Bryce, N. Ladommatos, H. Zhao, Appl. Opt. **39**, 27 (2000)

13. H. Bladh, J. Johnsson, P.-E. Bengtsson, Appl. Phys. B **90**, 1 (2008)

14. F. Migliorini, S. De Iuliis, S. Maffi, F. Cignoli, G. Zizak, Appl. Phys. B **96**, 4 (2009)

15. J. Zerbs, K.-P. Geigle, O. Lammel, J. Hader, R. Stirn, R. Hadef, W. Meier, Appl. Phys B **96**, 4 (2009)

16. B. Axelsson, R. Collin, P.-E. Bengtsson, Appl. Phys. B **72**, 3 (2001)

17. J.V. Pastor, J.M. Garcia, J.M. Pastor, J.E. Buitrago, Meas. Sci. Technol. **17**, 12 (2006)

18. A. Fuentes, G. Legros, H. El-Rabii, J.P. Vantelon, P. Joulain, J.L. Torero, Exp. Fluids **43**, 6 (2007)

19. R.L. Vander Wal, Proc. Combust. Inst. **27** (1998)

20. Y. Bouvier, C. Mihesan, M. Ziskind, E. Therssen, C. Focsa, J.F. Pauwels, P. Desgroux, Proc. Combust. Inst. **31** (2007)

21. P. Desgroux, X. Mercier, B. Lefort, R. Lemaire, E. Therssen, J.F. Pauwels, Combust. Flame **155**, 1 (2008)

22. R. Lemaire, A. Faccinetto, E. Therssen, M. Ziskind, C. Focsa, P. Desgroux, Proc. Combust. Inst. **32** (2009)

23. D.R. Snelling, G.J. Smallwood, F. Liu, Ö.L. Gulder, W.D. Bachalo, Appl. Opt. **44**, 31 (2005)

24. S. De Iuliis, F. Cignoli, G. Zizak, Appl. Opt. **44**, 34 (2005)

25. H. Bladh, J. Johnsson, P.-E. Bengtsson, Appl. Phys. B **96**, 4 (2009)

26. C.S. Moreau, E. Therssen, X. Mercier, J.F. Pauwels, P. Desgroux, Appl. Phys. B **78**, 3 (2004)

27. H.A. Michelsen, A.V. Tivanski, M.K. Gilles, L.H. van Poppel, M.A. Dansson, P.R. Buseck, Appl. Opt. **46**, 6 (2007)

28. D.R. Snelling, K.A. Thomson, F. Liu, G.J. Smallwood, Appl. Phys. B **96**, 4 (2009)

29. S. De Iuliis, F. Migliorini, F. Cignoli, G. Zizak, Proc. Combust. Inst. **31** (2007)

30. A. Boiarciuc, F. Foucher, C. Mounaïm-Rousselle, Appl. Phys. B **83**, 3 (2006)

31. J. Zerbs, K.P. Geigle, O. Lammel, J. Hader, R. Stirn, R. Hadef, W. Meier, Appl. Phys. B **96**, 4 (2009)

32. K.A. Thomson, M.R. Johnson, D.R. Snelling, G.J. Smallwood, Appl. Opt. **47**, 5 (2008)

33. J.R. Janesick, *Scientific Charge-Coupled Devices* (SPIE Optical Engineering Press, Bellingham, 2001)

34. D.R. Snelling, K.A. Thomson, G.J. Smallwood, Ö.L. Gülder, Appl. Opt. **38**, 12 (1999)

35. S. Trottier, H. Guo, G.J. Smallwood, M.R. Johnson, Proc. Combust. Inst. **31** (2007)

36. H.A. Michelsen, P.O. Witze, D. Kayes, S. Hochgreb, Appl. Opt. **42**, 27 (2003)

37. A.M. Law, J.S. Carson, Oper. Res. **27**, 5 (1979)

38. M. Schnaiter, H. Horvath, O. Mohler, K.-H. Naumann, H. Saathoff, O.W. Schock, J. Aerosol Sci. **34**, 10 (2003)

39. S.S. Krishnan, K.C. Lin, G.M. Faeth, J. Heat Transf. **122**, 3 (2000)

40. Ü.Ö. Köylü, G.M. Faeth, J. Heat Transf. **118**, 2 (1996)

41. A.R. Coderre, MASc dissertation, Carleton University, Canada, 2009

42. F. Liu, D.R. Snelling, K.A. Thomson, G.J. Smallwood, Appl. Phys. B **96** (2009)

43. T.C. Williams, C.R. Shaddix, Rev. Sci. Instrum. **78**, 12 (2007)

44. F. Liu, K.A. Thomson, G.J. Smallwood, J. Quant. Spectrosc. Radiat. Transf. **109** (2008)

45. K.J. Daun, K.A. Thomson, F. Liu, J. Heat Transfer **130** (2008)

46. F. Migliorini, S. DeIuliis, F. Cignoli, G. Zizak, Appl. Opt. **45**, 29 (2006)

47. D.R. Snelling, K.A. Thomson, G.J. Smallwood, Ö.L. Gülder, E.J. Weckman, R.A. Fraser, AIAA J. **40**, 9 (2002)